Atmospheric Environment 54 (2012) 746–753

Contents lists available at SciVerse ScienceDirect

Atmospheric Environment

journal homepage: www.elsevier.com/locate/atmosenv

An air pollution episode and its formation mechanism during the tropical cyclone Nuri's landfall in a coastal city of south China

John Xun Yang [a,1], Alexis Kai Hon Lau [a,b,*], Jimmy Chi Hung Fung [a,c], Wen Zhou [d], Mark Wenig [d]

[a] Division of Environment, The Hong Kong University of Science and Technology, Clear Water Bay, Kowloon, Hong Kong
[b] Department of Civil & Environmental Engineering, The Hong Kong University of Science and Technology, Clear Water Bay, Kowloon, Hong Kong
[c] Department of Mathematics, The Hong Kong University of Science and Technology, Clear Water Bay, Kowloon, Hong Kong
[d] School of Energy and Environment, City University of Hong Kong, Hong Kong

ARTICLE INFO

Article history:
Received 16 March 2011
Received in revised form
8 December 2011
Accepted 9 December 2011

Keywords:
Air pollution
Aerosol
Tropical cyclone
Remote sensing

ABSTRACT

In this work we investigated an air pollution episode during the landfall process of a tropical cyclone (TC) in Hong Kong. TCs affect air condition and account for most air pollution episodes in summer of this region. In August 2008, TC Nuri made direct landfall in Hong Kong. Before its landfall, an air pollution episode occurred, where major pollutants like SO_2 and PM_{10} increased eight and six times higher respectively. Rather than using single measurement method, we combined ground air sampling, lidar, sunphotometer and satellite lidar CALIPSO with focus on aerosol to study the episode mechanism, and some new phenomena were found. During the episode, it was found that heavy inland aerosol plumes existed in areas larger than urbanized regions and were elevated vertically and transported southward. During episode, planetary boundary layer (PBL) expansion and height increase were observed, which is different from previous reported PBL compression and height decrease. While vertical subsidence and horizontal stagnation and consequently local aerosol accumulation were attributed as the main episode cause in previous cases, our observation showed that transported aerosols dominated in this TC landfall event. This can be further confirmed by examining aerosol chemical composition, size distribution and single scattering albedo, where transported related species showed significantly change and local indicators remained relatively stable. Invigorated cloud droplets were found on the boundary layer top upon aerosol elevation. The results indicate that site difference and TC tracks should be considered for analyzing episode formation mechanism. They can cause difference in the strength of vertical subsidence and horizontal advection and affect pollution flow direction, which subsequently results in different pollution formation processes.

1. Introduction

Tropical cyclones (also known as hurricanes or typhoons) are powerful and destructive natural phenomena, affecting the atmospheric structure, constituents and human beings especially upon landfall. Recently the TC impact on air quality has drawn much attention. TCs can result in severe air pollution, especially in regions of frequent TC activities and heavy anthropogenic emissions like the western North Pacific and North Atlantic. In North Atlantic, there have been studies of TC activity and its interaction with aerosol (Cerveny and Balling, 1998). In western North Pacific, TC-caused heavy air pollution including high ozone and aerosol levels were reported (Huang et al., 2005, 2006; Lam et al., 2005; Wu et al., 2005; Feng et al., 2007; Wei et al., 2007; Fang et al., 2009; Fan et al., 2011). There have been either modeling (Huang et al., 2005; Feng et al., 2007) or observation-based studies of these phenomena. They include ground sampling (Fang et al., 2009) and satellite columnar observation (Badarinath et al., 2009), and they have investigated the evolution, cause and local-and-transport contributions of the TC-caused air quality change.

In China, the south China coast including the Pearl Delta River (PRD) region and Hong Kong are the mostly TC-affected regions (Zhang et al., 2009), where TC-caused air pollution is significant. Statistically, the TC related ozone episodes were found to account for the highest episode percentage (1/3 of all episodes) in Hong Kong (Huang et al., 2006). Furthermore, TCs account for most high aerosol episodes in summer seasons (Huang et al., 2009). Under TC

* Corresponding author. Institute for the Environment, The Hong Kong University of Science and Technology, Clear Water Bay, Kowloon, Hong Kong. Tel.: +852 23586944; fax: +852 23581582.
E-mail address: alau@ust.hk (A.K.H. Lau).
[1] Present address: Department of Atmospheric, Oceanic, and Space Sciences, The University of Michigan, Ann Arbor, USA

1352-2310/$ – see front matter © 2011 Elsevier Ltd. All rights reserved.
doi:10.1016/j.atmosenv.2011.12.023

favored synoptic conditions, high surface aerosol concentrations, low visibility and heavy aerosol loadings occurred (Wu et al., 2005; Wei et al., 2007; Feng et al., 2007; Badarinath et al., 2009). However, many studies were based on either modeling or a single measurement method and our knowledge on the episode formation mechanism is still limited for this reason.

In particular, several aspects need to be examined. The atmospheric vertical profile is important. The boundary layer is particularly related to pollution accumulation and episode formation. Horizontal advection can cause pollution dispersion and transport. For a specific site, the two factors together affect contribution from local and transported pollution. Aerosol chemical analysis and size distribution can make such discrimination. In the past, ground air samplings were carried out but chemical analysis was few and studies on aerosol pollution were limited. Although satellite columnar information was analyzed like using MODIS (Badarinath et al., 2009), large-scale observation and continuously vertical profile measurements were not found. Furthermore, while cases studies on TC of hundred kilometers away were reported, there are few studies on direct TC landfall events.

In this work we conducted a case study of TC Nuri, which made landfall in Hong Kong in August 2008. The purpose was to experimentally examine large-scale vertical and horizontal state and specific site situation so that the episode formation mechanism could be investigated. It was fulfilled by combining measurements from satellite and ground remote sensing, ground air sampling and aerosol chemical analysis. Results different from previous studies were found such as the extensive elevated aerosols and increased PBL height. While subsidence and stagnation were attributed as the main cause of aerosol increase in the past, transported aerosol dominated in Hong Kong in this case. The TC landfall caused pollution episode differs from cases where TC centers were several hundred kilometers away. The study suggests that the site and TC track difference need to be accounted for explaining episode mechanism.

2. Data and methodology

2.1. Measurement location and period

In August 2008, Tropical Cyclone Nuri made landfall in Hong Kong (UTC+8). Nuri was first formed in the western North Pacific at ~14.3 N and 148 E, initiated from a tropical disturbance. It became a tropical storm on 16 August. After several days, it developed into a strong tropical cyclone and reached typhoon strength between 19 and 22 August. It then moved northwesterly through the ocean north of The Philippines and entered the South China Sea. On 21 August, it approached the south china coast and made landfall, heading directly to Hong Kong on 22 August at ~15:00 local time. Nuri necessitated the issuance of the first No. 9 TC warning signal in Hong Kong since 2003. Afterwards it moved northwesterly into the inland and dissipated. Fig. 1 shows Nuri's six-hourly best track according to the Joint Typhoon Warning Center (JTWC). During the TC's passage through Hong Kong, continuous ground-based measurements have been made. An elastic scattering lidar was installed in the Yuen Long (22.26° N, 114.50° E) site for 24-h monitoring, and corresponding meteorological conditions were also recorded. With the ground lidar, atmospheric vertical profile can be measured and PBL height was retrieved. Air sampling of atmospheric constituents was performed including hourly SO_2, NO_x, NO_2, $PM_{2.5}$ and PM_{10}. A sunphotometer installed in the main campus of City University of Hong Kong was utilized. Data from satellite CALIPSO were used for studying atmospheric vertical profile. The true color satellite images were from the Moderate Resolution Imaging Spectroradiometer (MODIS).

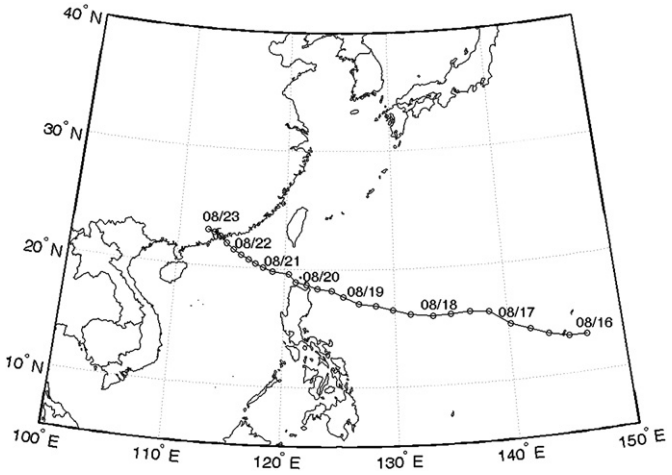

Fig. 1. The tropical cyclone Nuri's best track observed every 6 h at the Joint Typhoon Warning Center.

2.2. Satellite lidar CALIPSO

For our purpose of large-scale vertical profile examination, the Cloud-Aerosol Lidar with Orthogonal Polarization (CALIOP) is very useful as its polarization property can discriminate spherical and non-spherical cloud and aerosol particles (Winker et al., 2007; Liu et al., 2009). The CALIOP is on board the Cloud-Aerosol Lidar and Infrared Pathfinder Satellite Observations (CALIPSO) satellite, launched on 23 April 2006. CALIPSO runs on a sun-synchronous orbit and has a 16-day repeat cycle. Its main instrument is based on a Nd:YAG laser operating at 1064 and 532 nm. The laser has a repetition frequency of ~20.16 Hz and therefore produces around every 330 m footprints on the ground track. The emitted laser beam is linearly polarized, but the depolarization measurements are only made at the 532 nm channel where the backscatter signals are separated into polarized parallel and perpendicular beams with respect to the outgoing beams. The parallel and perpendicular backscatter signals together can discriminate the spherical and non-spherical aerosol and cloud particles. Non-spherical objects like thin cirrus and dust produce strong depolarized backscatter signals in the perpendicular channel, while spherical particles like anthropogenic aerosols cause little depolarized signals. Thick clouds of spherical droplets produce even stronger depolarized perpendicular signals due to multiple scattering.

The CALIPSO level-1 attenuated backscatter data was used. The vertical resolutions are 0.33, 0.33, 1.0, 1.67 and 5.0 km for the altitude ranges of ~0.5–8.2, 8.2–20.2, 20.2–30.1, 30.1–40.0 km, respectively, and the corresponding horizontal resolutions are 30, 60, 180 and 300 m. We averaged the dataset to have a 5-km horizontal resolution. In fact, we also looked at other dataset like the level-2 vertical feature dataset derived from the level-1 data (Liu et al., 2009). We found that for our purpose the level-1 dataset show more details about aerosol and clouds. For example, as can be seen in Fig. 2, backscatter signals are colored according to their strength increasing from blue to gray. For the total attenuated backscatter, the gray scale usually denotes the strong backscatter signals from the surface and clouds, and yellow and red scales denote returning signals from weak clouds and strong aerosols, and green and blue show the molecular backscatter or weak aerosols and clouds (Winker et al., 2007). In perpendicular backscatter, aerosols and clouds produce weak and strong signals respectively. Furthermore, dust plumes are rare in TC seasons in south China and therefore backscatter signals in the perpendicular channel indicate clouds rather than dust.

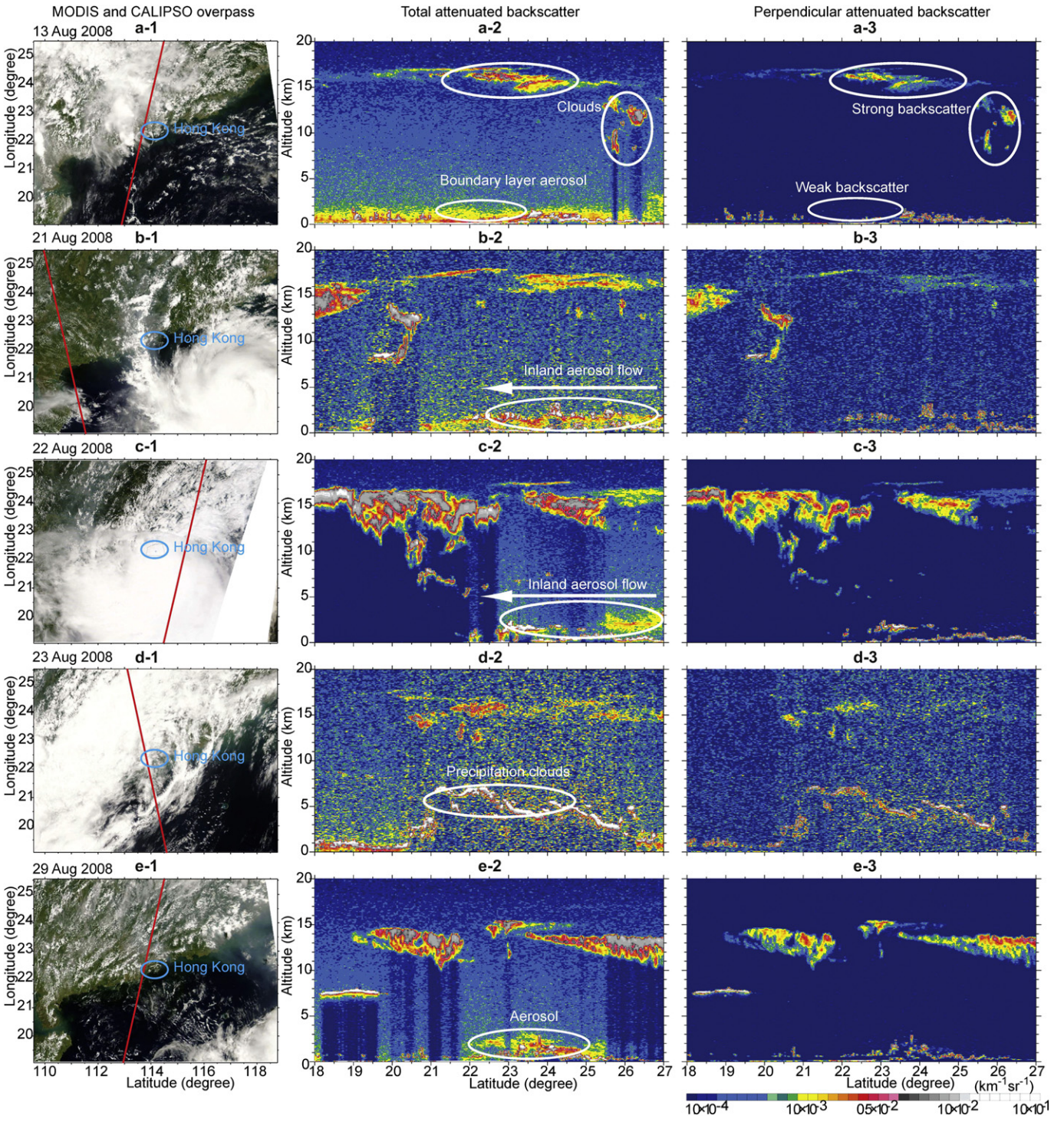

Fig. 2. The satellite observations from the MODIS and CALIPSO. The rows correspond to different days and columns show MODIS images (1st columns), CALIPSO vertical profiles of the total attenuated backscatter (2nd columns) and perpendicular backscatter (3rd columns), respectively. Red lines denote CALIPSO tracks. The highlighted circles denote aerosols and clouds respectively, which can be discriminated using CALIPSO's two profiles where in the perpendicular profile cloud droplets cause strong backscatter and aerosols cause weak backscatter. It is found that elevated extensive aerosol plumes transported southerly and clouds were invigorated mixed with aerosols. (For interpretation of the references to colour in this figure legend, the reader is referred to the web version of this article.)

2.3. Ground remote sensing

The continuous ground lidar observation is necessary since satellite lidar overpass is limited. It was an elastic micro-pulse 523 nm Nd: YLF lidar, manufactured by Sigma Space Corp. of model 1000 and had a pulse repetition rate of 2500 Hz and duration of 200 ns with vertical resolution of 30 m. Data was recorded every 15-s for 24-h monitoring. We averaged the data of every 15-m. The lidar alignment has been performed and more instrument specification and alignment details can be found in the earlier paper (He et al., 2006). For determining the PBL height, we adopted the method mainly based on studying the gradient of range-corrected

backscatter. This method assumes that atmospheric constituents are mainly within the boundary layer and sharp drop at the PBL top is expected (Hennemuth and Lammert, 2006; Wiegner et al., 2006).

The atmospheric columnar aerosol was measured by using a sunphotometer (Yang and Wenig, 2009), which provided useful information on aerosol size distribution, single scattering albedo (SSA) and aerosol optical depth (AOD). It has seven spectral channels with centered wavelengths at 315, 400, 500, 675, 870, 940, and 1020 nm respectively. The 315 and 940 nm channels are used for deriving the ozone concentration and precipitable water column amounts, respectively, while the other five wavelengths are used for measuring aerosols. It operated automatically 24-h each day with valid performance in daytime. By measuring the direct and diffused solar radiation, columnar aerosol optical properties can be retrieved. The cloud can often influence the measurement and contaminate the data. A cloud screening algorithm was adopted (Smirnov et al., 2000) and several constraining methods were used (Yang and Wenig, 2009).

2.4. Air sampling and aerosol chemical analysis

Ground aerosol measurements and chemical composition analysis allow for examining essential aerosol characteristics and source apportionment. Air sampling was conducted at the Yuen Long site and was the regular measurement operated by Hong Kong Environmental Protection Department (Yuan et al., 2006; HKEPD, 2003). The detailed sampling methods are introduced here. Instruments were installed at the building roof around 25 m from the ground so that road dust does not affect observations significantly at this elevation. Hourly particulate matter PM_{10} and PM_2, particulates with aerodynamic diameter less than 10 and 2.5 m respectively, were measured as well as gaseous pollutants including SO_2, NO_x, NO_2 and O_3. The PM_{10} and $PM_{2.5}$ Tapered Element Oscillating Microbalance monitors were used. They are gravimetric instruments using the Teflon-coated borosilicate glass filter for measuring real-time aerosol mass concentrations. The sample stream was heated to 50° before entering the mass transducer for humidity control. Furthermore, chemical analysis of 24-h sampled PM_{10} was carried out every 6-days. The Graseby-Anderson high volume sampler was used for collecting 24-h PM. The control limits for the PM measurements are 10% for both accuracy and precision. The organic and elemental carbon (OC & EC) were measured using a thermal/optical transmittance method. The analysis protocol followed the NIOSH method 5040 (Birch and Cary, 1996). Sin et al. (2002) discussed detail analytical procedure. Yu et al. (2004) and Lee et al. (2006) discussed the OC artifacts. For PM_{10} chemical analysis, twenty-six element and water-soluble ions were analyzed. USEPA IO-3 method with two analysis techniques was used for metallic species (USEPA, 2003). Inductively coupled plasma atomic emission spectroscopy (ICP-AES) was used for Aluminum (Al), Barium (Ba), Beryllium (Be), Calcium (Ca), Cadmium (Cd), Chromium (Cr), Copper (Cu), Iron (Fe), Magnesium (Mg), Manganese (Mn), Nickel (Ni), Lead (Pb), Vanadium (V) and Zinc (Zn) measurement. The flow injection analysis atomic absorption was used for Arsenic (As), Mercury (Hg) and Selenium (Se). Ion chromatography was used for measuring water-soluble species including sulfate (SO_4^{2-}), nitrate (NO_3^-), chloride (Cl^-), Bromin (Br^-), ammonium ion (NH_4^+), sodium (Na^+) and potassium (K^+).

Reconstructing aerosol chemical composition was performed to better understand aerosol composition as well as to support source apportionment. The method is briefly introduced here. Following previous studies, the basic idea is analyzing chemical molar structure with necessary empirical parameter adjustment due to consideration like region and source specification (Malm et al., 1994; Landis et al., 2001; Ho et al., 2003; Yu et al., 2004; Andreae et al., 2008; Hsu et al., 2010). For sulfate, the method used the relation Sulfate $= SO_4^{2-} - 0.252Na$, so as to eliminate the impact of sea-salt sulfate (Ho et al., 2003). Dust levels were estimated using combined trace elements (Malm et al., 1994). Since we did not analyze elements like Ti and Si, an alternative method was used as, Dust $= 12.5Al$, which has been used in this region Andreae et al., 2008. Sea salt was calculated as Sea-salt $= 2.54Na$ (Malm et al., 1994; Ho et al., 2003). Particulate organic matter (POM) was estimated as, $POM = 2.2OC$ (Yu et al., 2004), where the value corresponds to inland air flow to Hong Kong which is the case under the TC-caused counter-clockwise flow. The trace element oxides (TEO) contain major heavy metals and were calculated as, $TEO = 1.47V + 1.29Mn + 1.27Ni + 1.25Cu + 1.24Zn + 1.32As + 1.08Pb + 1.20Se + 1.37Sr + 3.07P + 1.31Cr + 1.41K$ (Landis et al., 2001) with all available element data we had. Nitrate and ammonium were specified separately using measured NO_3^- and NH_4^+, respectively.

3. Results and discussion

3.1. Atmospheric vertical profile

The critical atmospheric vertical profile was examined using satellite and ground lidar, which presented the first large-scale and continuous ground monitoring in this region. A series of satellite observations are shown in Fig. 2, where row panels represent different times and column panels represent different channels. The situation before the TC on 13 August is shown in the first row. Fig. 2a-1 shows the MODIS Aqua image from its visible channel, and the CALIPSO track is denoted as the red line. The CALIPSO flight direction was from north to south during local daytime and south to north at nighttime. There was a time difference between the MODIS and CALIPSO passing times but the time lag was short, so the synoptic conditions did not change significantly. Fig. 2a-2 and 2a-3 show the total attenuated backscatter and perpendicular backscatter respectively. The two channels together can well discriminate aerosol and cloud particles, where strong perpendicular signals indicate depolarizing from non-spherical backscatter like thin cirrus or thick clouds droplets due to multiple scattering while aerosols produce little signal in perpendicular channel. The highlighted cirrus up to 16–17 km were located over the south China coast region. The cirrus caused strong signals in the both channels. In contrast, aerosol layer beneath the cirrus as highlighted by red circle is almost non-depolarizing and produces very weak signals in the perpendicular profile. This is a useful key feature of CALIPSO, while previous non-polarization lidars cannot discriminate aerosol and cloud experimentally. Before the TC, aerosols were mainly within boundary layer of height below 1 km.

On 21 August, the TC already entered the South China Sea and its periphery affected the south China coastal regions. Fig. 2b-1 shows the satellite image. In regions with latitude lower than 19° N, the TC's cirrus shield came to ~16 km and had a thickness of ~5 km producing strong backscatter in both channels as in Fig. 2b-3. Different from before-TC state where most aerosols attached close to the ground surface, aerosol lifting can be seen as in highlighted circle of Fig. 2b-2. Aerosols showed obvious lifting and updraft beyond previous 1 km. This is different from vertical subsidence cases where boundary layer compression and consequently aerosol accumulation were reported (Wu et al., 2005; Feng et al., 2007; Fan et al., 2011). With the aerosol lifting, there cloud droplets were invigorated and mixed with aerosols. This can be found by the strong backscatter in both total attenuation and perpendicular channels.

As the TC approached, the 22 August situation is shown in Fig. 2c. Although thick cloud shield prevented satellite penetrating into the

lower atmosphere, clear profiles were obtained in cloud broken regions due to TC spiral periphery. The aerosol lifting was clear. In regions like ~25–27° N, abundant aerosols were found and they lifted to a height of 2 km. Previous studies did not show heavy aerosols in this region. The urbanized Guangzhou region were attributed as the source where pollutions accumulated and increased upon TC impact (Wu et al., 2005; Feng et al., 2007). However, vertical profiles here showed aerosol existence much larger than urbanized PRD center. Furthermore, accompanying with aerosol lifting, more cloud droplets at heights of ~2 km were found like in regions of ~22–24° N.

Regarding the horizontal advection, it is clear from satellite observations that those inland pollutants were horizontally advected from north to south. The northward moving TC-caused horizontal advection to TC center and thus drew air flow from north to Hong Kong. This can be also found in later ground site observation. On 23 August right after the TC landfall, much precipitation took place with a maximum amount of ~10 mm h^{-1}. The CALIPSO overpass showed a dense precipitating cloud belt at a height of ~4–6 km as in Fig. 2d-2. On 29 August, the TC had dissipated and atmospheric conditions were gradually restored. However, aerosol vertical lifting remained strong and came to ~3 km.

In addition to CALIPSO, we employed a continuous ground lidar, which is necessary since satellite lidar was limited by a 16-day repeat orbit cycle and clouds can prevent it from detecting the lower atmosphere condition. Fig. 3 shows time series of the normalized attenuated backscatter, where the dashed line denotes the identified PBL height. Panel 5 of Fig. 4 also shows times series of hourly mean temperature and PBL height. It is found that the PBL height demonstrates daily variation subject to the temperature change. The temperature led about 2 h ahead of PBL height. It is obvious that PBL height increased during the episode from 20 to 21 August, and stronger backscattering occurred due to increasing aerosols. The average PBL heights were 0.94 km from 14 to 18 August, 1.22 km during episode from 20 to 21 August and 0.92 km from 25 to 28 August respectively. Strong backscatter can be seen at the PBL top, which was probably due to cloud droplets and agreed with satellite observation. These results are in contrast with previous cases where PBL compression was reported (Wu et al., 2005; Feng et al., 2007; Fan et al., 2011). PBL compression generally corresponds to aerosol increasing, however, in this event, PBL did not compress but instead expanded and aerosol concentration stilled increased. After TC landfall, air flow direction changed to southerly. The PBL decreased and collapsed dramatically with a minimum of 0.34 km. Strong backscatter up to 5–7 km was observed due to cloud droplets, showing agreement with satellite observation. From 24 August, atmospheric vertical profile gradually restored to the start state.

The PBL height increase can come from both atmospheric vertical motion and horizontal warm air flow advected from inland region to Hong Kong. The temperature in inland regions was high and corresponding air flows to Hong Kong were warmer. Also, this TC landfall case differs from those when TCs were hundreds of kilometers away from observation sites and horizontal advection was relatively weak. It implies TC tracks can make different impact. TC tracks change can consequently change the strength of vertical and horizontal motion and air flow direction. The TC track distance from observation site and TC moving direction can cause difference. In fact, one earlier ground air sampling measurements showed difference under several consecutive TC impacts (Fang et al., 2009). Furthermore, invigorated cloud droplets were found upon aerosol lifting, which might be due to the fact that aerosol can serve as cloud condensation nuclei (CCN). Regarding aerosol lifting, we do not have a convincing explanation yet, but there were modeling studies showing aerosol radiative and microphysical properties might account (Rosenfeld et al., 2007; Zhang et al., 2007; Khain et al., 2008).

3.2. Atmospheric constituents and aerosol evolution

We looked into ground air sampling measurements and examined aerosol properties. Fig. 4 shows the time series of weather conditions and atmospheric constituents. Before the TC, gas pollutants of SO_2, NO_2, NO_x and O_3 were 19, 33, 69 and 21 g m^{-3} from 14 to 18 August, respectively. NO_2, NO_x and O_3 rendered daily variation patterns probably related to atmospheric conditions like solar radiation and temperature. Before the episode, the prevailing wind was from southeast direction. The Pollution episode started on 20 August when the four pollutants rose as high as 157, 147, 218 and 210 g m^{-3} respectively. In the meantime, wind direction changed northwesterly in contrast to earlier southwesterly wind. Wind speed did not show much change and thus the stagnation effect was not pronounced. This suggests that transport is major

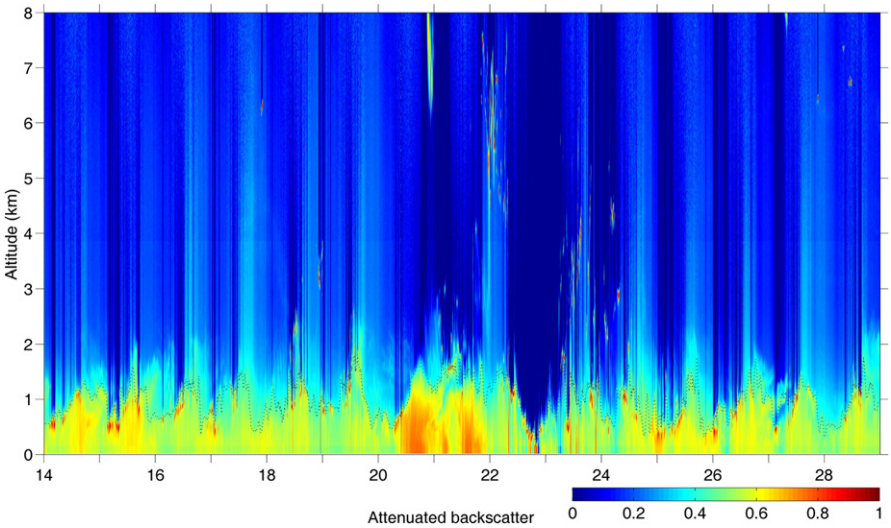

Fig. 3. Time series of attenuated backscatter from ground lidar. The dashed line denotes the PBL height. PBL expansion and height increase were observed during pollution episode.

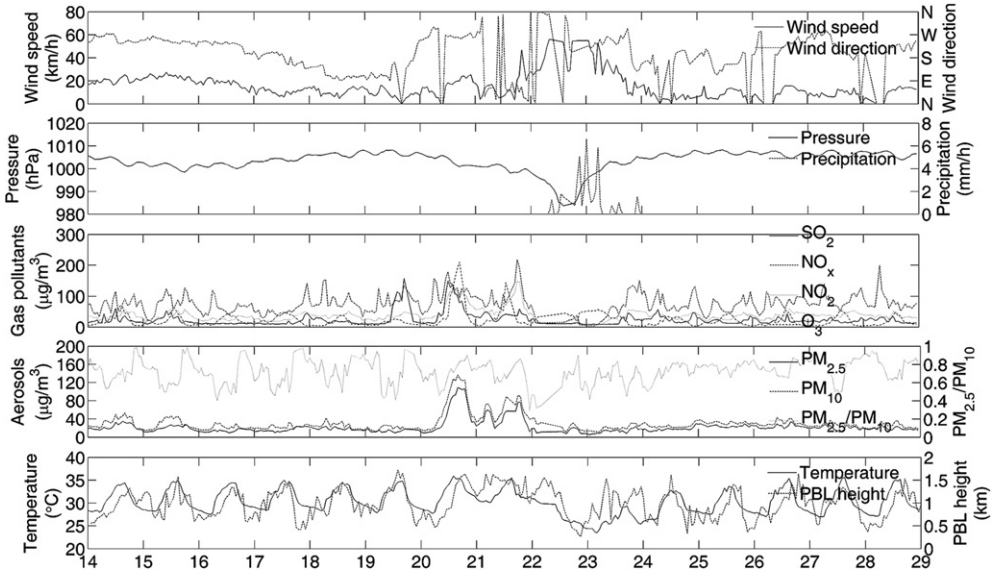

Fig. 4. Time series of hourly mean atmospheric conditions throughout the TC landfall. The PBL height in Panel 5 is from ground lidar retrieval. Significant pollution increase was found on episode and PBL height also increased.

contribution of pollution increase compared to local accumulation. It differs from situation from further inland regions where stagnation and boundary compression were attributed as main reason of aerosol increase (Wu et al., 2005; Fan et al., 2011).

The TC induced aerosol change was significant. Before the TC, aerosol concentrations were low and did not have pronounced daily variation. Coinciding with wind direction change, PM_2 and $PM_{2.5}$ increased and came to as high as 137 and 109 g m^{-3} on 20 August, six and five times higher than before-TC levels when they were 26 and 17 g m^{-3} from 14 to 18 August, respectively. The significant aerosol increase supported the observed vertical profiles of abundant aerosol plumes inland. The ratios of $PM_{2.5}$ to PM_{10} were 0.69, 0.64 and 0.71 before, during and after TC, respectively. Since anthropogenic aerosol levels were heavy in this region, the ratio did not show pronounced change, thus chemical analysis can better examine aerosol properties.

Fig. 5 shows the aerosol chemical composition data on 14, 20 and 26 August that represented the before-TC, episode and after-TC conditions respectively. Before the TC, POM contributes mostly in composing PM_{10}, and components including sulfate, dust, EC and sea salt are also important contributors. The composition is consistent with previous studies on local aerosol (Ho et al., 2003) but showed higher POM percentage. In inland PRD cities, high POM was reported (Andreae et al., 2008). During episode, species including ammonium, sulfate, POM, TEO and EC increased 5.65, 3.15, 1.8, 1.8 and 1.14 times, respectively. The unidentified species also increased due to more complicated aerosol conditions and instrument limitation. Compositions including sea salt, dust and nitrate decreased slightly as 0.85, 0.83 and 0.73 compared to that on 14 August. In terms of percentage change, sulfate and ammonium increased as 1.58 and 2.82 times higher, while other species decreased slightly. The EC increase was not pronounced while species including POM, sulfate and ammonium increases were much larger. Since EC is more related to local emission, the results indicate that transported pollutants were major cause of this pollution episode.

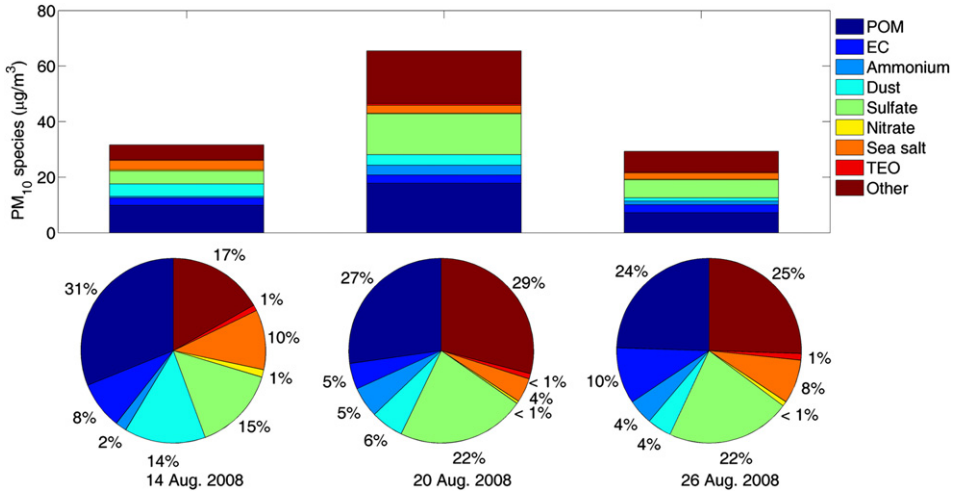

Fig. 5. Chemical compositions of ground measured PM_{10} on before-TC (18 August), episode (20 August) and after TC (26 August) days respectively. Transport related aerosol species like POM and sulfate showed significantly increase on episode and decrease after TC, while local indicator like EC did not change a lot relatively.

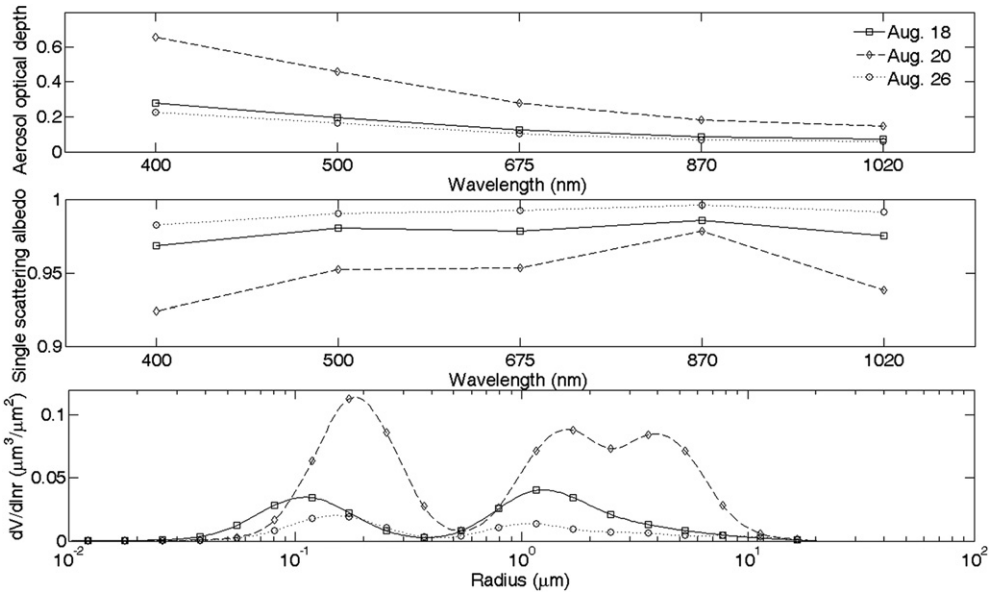

Fig. 6. The columnar atmospheric aerosol conditions in terms of aerosol optical depth (a) single scattering albedo (b) and size distribution (c). SSA decreased due to more absorbing aerosols and size distribution increased and shifted to larger size, which indicates impact of transported aerosol.

After TC landfall, all aerosol species decreased. Their amounts dropped to 0.40, 0.97, 0.43, 0.37, 0.80, 0.57, 0.33, 0.81 and 0.39 for POM, EC, sulfate, ammonium, nitrate, TEO, dust and sea salt, respectively. This was because heavy precipitation and later southerly wind from the ocean as the TC entered inland. Again, EC change was relatively small in comparison to more transport related indicators like POM. Comparing before and after TC states, aerosol compositions showed difference. After TC, species including EC, ammonium, sulfate, TEO were at a little higher level of 1.1, 2.1, 1.36, 1.03 times larger, while POM, nitrate, dust and sea salt decreased to 0.73, 0.59, 0.28, 0.68 times respectively. Due to TC heavy precipitation, air became clean in general. However, high EC, ammonium and sulfate indicate local emission. Ho et al. (2003) suggested that sulfate was one major constituent in background site of Hong Kong. In particular, local power plants and vehicle emissions might be contributor (Yu et al., 2004; Yuan et al., 2006; Lee et al., 2006).

We further examined aerosol size distribution, SSA and AOD. Fig. 6 shows columnar aerosol information on 14, 20 and 28 August respectively. Because measurement condition limitations like the cloud contamination, the available data did not completely coincide with other measurements. Although sunphotometer was continuously operated, TC cloud shield always affected measurements. We examined TC approaching events in past three years, and this time has relatively good observing weather conditions. During episode, AOD increased to 2.34 times high on 20 August as 0.66 at 467 nm wavelength and SSA dropped from 0.97 to 0.92. The SSA decrease indicates more absorbing aerosol. This implies inland aerosol transport since high pollution levels including black carbon were found in northwestern PRD region (Andreae et al., 2008).

Combining aerosol chemical analysis, the size distribution provided useful information, which was not reported in previous TC-caused episodes. The measured aerosol size distribution had a bimodal structure with fine mode at ~0.01–0.6 m and the coarse mode at ~0.6–15 m. This bimodal size distribution was reported before (Dubovik et al., 2002; Yang and Wenig, 2009). During the pollution episode, aerosol increase happened in almost the whole size range. The overall aerosol size shifted to larger size. The median volume radii were 0.53, 0.85, 0.54 m respectively throughout the TC landfall. The size distribution change reflects a comparison of inland and local aerosol and indicates the existence of transported aerosols. Following the formula for characterizing aerosol size distribution (Dubovik et al., 2002), the volume fraction of $PM_{2.5}$ to PM_{10} was 0.60, 0.50 and 0.66, which was consistent with the air sampling measured mass fraction in the daytime as 0.65, 0.62 and 0.70 respectively in Fig. 4. The size distribution indicates that fine aerosol like $PM_{2.5}$ contributed a lot in this region. While chemical analysis found POM, EC, sulfate, dust and sea salt contribute more than 70% mass composition, the size distribution implies that POM, EC and sulfate were abundant in fine mode, and that dust and sea salt would present in coarse mode.

4. Conclusions

A TC-caused pollution episode has been investigated using multiple measurement tools. The consistent experimental results show different episode formation mechanism from previous cases. The existence of large-scale inland heavy aerosol plumes and corresponding elevation and outflows were revealed from satellite observation. Heavy pollution plumes existed in areas much larger than urbanized PRD center. Aerosol lifting was found despite subsidence motion in TC periphery and corresponding cloud droplets were invigorated at the boundary layer top. Aerosols from horizontal advection dominated aerosol increase in this episode at Hong Kong, which shows difference from inland sites where stagnation and subsidence were attributed as the main cause for aerosol accumulation. Meanwhile, PBL expansion was found in contrast with compression. Aerosol increase was associated with PBL expansion while previously aerosol increase was accompanied by PBL compression. Ground measured aerosol chemical species, SSA and size distribution confirmed the impact of transported aerosols. There was significantly change in transported species while local related pollutants relatively kept stable. The results suggest that site difference need to be considered when investigating pollution formation mechanism. In sites of heavy emission sources, local aerosol accumulation can contribute significantly in episode. Furthermore, it implies that TC tracks can cause difference. When TC centers were hundreds of kilometers far away rather than making direct landfall, subsidence and stagnation were reported as main pollution cause. Different TC tracks can change the strength of vertical subsidence and horizontal advection and vary pollution

transport direction, thus pollution formation process can be different.

Acknowledgments

We appreciate Hong Kong Environmental Protection Department (HKEPD) for providing the air quality monitoring data, Hong Kong Observatory (HKO) for providing the meteorological data, and support from FU TAK IAM FOUNDATION (FTI) project, HKUST SRFIPO01 and our joint funding from NSFC-GD (U1033001). We thank the grant from CityU Project 7002458.

References

Andreae, M.O., Schmid, O., Yang, H., Chand, D., Yu, J.Z., Zeng, L.M., Zhang, Y.H., 2008. Optical properties and chemical composition of the atmospheric aerosol in urban Guangzhou, China. Atmospheric Environment 42 (25), 6335–6350.

Badarinath, K.V.S., Kharol, S.K., Sharma, A.R., Ramaswamy, V., Kaskaoutis, D.G., Kambezidis, H.D., 2009. Investigations of an intense aerosol loading during 2007 cyclone SIDR – a study using satellite data and ground measurements over Indian region. Atmospheric Environment 43 (24), 3708–3716.

Birch, M.E., Cary, R.A., 1996. Elemental carbon-based method for monitoring occupational exposures to particulate diesel exhaust. Atmospheric Environment 25, 221–241.

Cerveny, R.S., Balling, R.C., 1998. Weekly cycles of air pollutants, precipitation and tropical cyclones in the coastal NW Atlantic region. Nature 394 (6693), 561–563.

Dubovik, O., Holben, B., Eck, T.F., Smirnov, A., Kaufman, Y.J., King, M.D., Tanre, D., Slutsker, I., 2002. Variability of absorption and optical properties of key aerosol types observed in worldwide locations. Journal of the Atmospheric Sciences 59 (3), 590–608.

Fan, S.J., Fan, Q., Yu, W., Luo, X.Y., Wang, B.M., Song, L.L., Leong, K.L., 2011. Atmospheric boundary layer characteristics over the Pearl River Delta, China, during the summer of 2006: measurement and model results. Atmospheric Chemistry and Physics 11 (13), 6292–6310.

Fang, G.C., Lin, S.J., Chang, S.Y., Chou, C.C.K., 2009. Effect of typhoon on atmospheric particulates in autumn in central Taiwan. Atmospheric Environment 43 (38), 6039–6048.

Feng, Y.R., Wang, A.Y., Wu, D., Xu, X.D., 2007. The influence of tropical cyclone Melor on PM_{10} concentrations during an aerosol episode over the Pearl River Delta region of China: numerical modeling versus observational analysis. Atmospheric Environment 41 (21), 4349–4365.

He, Q.S., Li, C.C., Mao, J.T., Lau, A.K.H., Li, P.R., 2006. A study on the aerosol extinction-to-backscatter ratio with combination of micro-pulse LIDAR and MODIS over Hong Kong. Atmospheric Chemistry and Physics 6, 3243–3256.

Hennemuth, B., Lammert, A., 2006. Determination of the atmospheric boundary layer height from radiosonde and lidar backscatter. Boundary-Layer Meteorology 120 (1), 181–200.

Ho, K.F., Lee, S.C., Chan, C.K., Yu, J.C., Chow, J.C., Yao, X.H., 2003. Characterization of chemical species in $PM_{2:5}$ and PM_{10} aerosols in Hong Kong. Atmospheric Environment 37 (1), 31–39.

Hong Kong Environmental Protection Department, 2003. Air Quality in Hong Kong 2002. http://www.epd.gov.hk/epd/english/environmentinhk/air/airquality/files/aqr02e.pdf.

Hsu, S.C., Liu, S.C., Tsai, F., Engling, G., Lin, I., Chou, C.K.C., Kao, S.J., Lung, S.C.C., Chan, C.Y., Lin, S.C., Huang, J.C., Chi, K.H., Chen, W.N., Lin, F.J., Huang, C.H., Kuo, C.L., Wu, T.C., Huang, Y.T., 2010. High wintertime particulate matter pollution over an offshore island (Kinmen) off_ southeastern China: an overview. Journal of Geophysical Research-Atmospheres 115, D17309.

Huang, J.P., Fung, J.C.H., Lau, A.K.H., 2006. Integrated processes analysis and systematic meteorological classification of ozone episodes in Hong Kong. Journal of Geophysical Research-Atmospheres 111, D20309.

Huang, J.P., Fung, J.C.H., Lau, A.K.H., Qin, Y., 2005. Numerical simulation and process analysis of typhoon-related ozone episodes in Hong Kong. Journal of Geophysical Research-Atmospheres 110, D05301.

Huang, X.F., Yu, J.Z., Yuan, Z.B., Lau, A.K.H., Louie, P.K.K., 2009. Source analysis of high particulate matter days in Hong Kong. Atmospheric Environment 43 (6), 1196–1203.

Khain, A., Cohen, N., Lynn, B., Pokrovsky, A., 2008. Possible aerosol effects on lightning activity and structure of hurricanes. Journal of the Atmospheric Sciences 65 (12), 3652–3677.

Lam, K.S., Wang, T.J., Wu, C.L., Li, Y.S., 2005. Study on an ozone episode in hot season in Hong Kong and transboundary air pollution over Pearl River Delta region of China. Atmospheric Environment 39 (11), 1967–1977.

Landis, M.S., Norris, G.A., Williams, R.W., Weinstein, J.P., 2001. Personal exposures to $PM_{2:5}$ mass and trace elements in Baltimore, MD, USA. Atmospheric Environment 35 (36), 6511–6524.

Lee, S.C., Cheng, Y., Ho, K.F., Cao, J.J., Louie, P.K.K., Chow, J.C., Watson, J.G., 2006. $PM_{1:0}$ and $PM_{2:5}$ characteristics in the roadside environment of Hong Kong. Aerosol Science and Technology 40 (3), 157–165.

Liu, Z.Y., Vaughan, M., Winker, D., Kittaka, C., Getzewich, B., Kuehn, R., Omar, A., Powell, K., Trepte, C., Hostetler, C., 2009. The CALIPSO lidar cloud and aerosol discrimination: version 2 algorithm and initial assessment of performance. Journal of Atmospheric and Oceanic Technology 26 (7), 1198–1213.

Malm, W.C., Sisler, J.F., Huffman, D., Eldred, R.A., Cahill, T.A., 1994. Spatial and seasonal trends in particle concentration and optical extinction in the United-States. Journal of Geophysical Research-Atmospheres 99 (D1), 1347–1370.

Rosenfeld, D., Khain, A., Lynn, B., Woodley, W.L., 2007. Simulation of hurricane response to suppression of warm rain by sub-micron aerosols. Atmospheric Chemistry and Physics 7 (13), 3411–3424.

Sin, D.W.M., Fung, W.H., Lam, C.H., 2002. Measurement of carbonaceous aerosols: validation and comparison of a solvent extraction-gas chromatographic method and a thermal optical transmittance method. Analyst 127, 614–622.

Smirnov, A., Holben, B.N., Eck, T.F., Dubovik, O., Slutsker, I., 2000. Cloud-screening and quality control algorithms for the AERONET database. Remote Sensing of Environment 73 (3), 337–349.

US Environmental Protection Agency, Office of Research and Development, 2003. Compendium Method IO-3: Chemical Species Analysis of Filter-Collected Suspended Particulate Matter (SPM). http://www.epa.gov/ttn/amtic/inorg.html.

Wei, X.L., Li, Y.S., Lam, K.S., Wang, A.Y., Wang, T.J., 2007. Impact of biogenic voc emissions on a tropical cyclone-related ozone episode in the Pearl River Delta region, China. Atmospheric Environment 41 (36), 7851–7864.

Wiegner, M., Emeis, S., Freudenthaler, V., Heese, B., Junkermann, W., Munkel, C., Schafer, K., Seefeldner, M., Vogt, S., 2006. Mixing layer height over Munich, Germany: variability and comparisons of different methodologies. Journal of Geophysical Research-Atmospheres 111, D13201.

Winker, D.M., Hunt, W.H., McGill, M.J., 2007. Initial performance assessment of CALIOP. Geophysical Research Letters 34, L19803.

Wu, D., Tie, X.X., Li, C.C., Ying, Z.M., Lau, A.K.H., Huang, J., Deng, X.J., Bi, X.Y., 2005. An extremely low visibility event over the Guangzhou region: a case study. Atmospheric Environment 39 (35), 6568–6577.

Yang, X., Wenig, M., 2009. Study of columnar aerosol size distribution in Hong Kong. Atmospheric Chemistry and Physics 9 (16), 6175–6189.

Yu, J.Z., Tung, J.W.T., Wu, A.W.M., Lau, A.K.H., Louie, P.K.K., Fung, J.C.H., 2004. Abundance and seasonal characteristics of elemental and organic carbon in Hong Kong PM_{10}. Atmospheric Environment 38 (10), 1511–1521.

Yuan, Z.B., Lau, A.K.H., Zhang, H.Y., Yu, J.Z., Louie, P.K.K., Fung, J.C.H., 2006. Identification and spatiotemporal variations of dominant PM_{10} sources over Hong Kong. Atmospheric Environment 40 (10), 1803–1815.

Zhang, H., McFarquhar, G.M., Saleeby, S.M., Cotton, W.R., 2007. Impacts of Saharan dust as CCN on the evolution of an idealized tropical cyclone. Geophysical Research Letters 34, L14812.

Zhang, Q.A., Wu, L.G., Liu, Q.F., 2009. Tropical cyclone damages in China 1983–2006. Bulletin of the American Meteorological Society 90, 489–495.